Spitzer observations of WASP-17b

David Anderson & Alexis Smith

(Keele University)

dra@astro.keele.ac.uk

amss@astro.keele.ac.uk

Travis Barman (Lowell Observatory), Andrew Cameron (Univ. of St. Andrews), Joe Harrington (UCF), Peter Wheatley (Univ. of Warwick)

Abstract

We present *Spitzer*/IRAC observations of the occultation (secondary eclipse) of WASP-17b at 4.5 and 8 μm. Our global analysis of these data, together with transit photometry and radial velocities, reveals an orbital eccentricity close to zero (0.035±0.013), and a planet radius of 2.00 R_J, meaning WASP-17b is the largest known exoplanet.

We show that it is necessary to detrend 8 μm data with detector position, a technique which is not part of any analysis reported in the literature. We caution that failure to treat this effect, and to optimise the photometric aperture size, can have a significant impact on the eclipse depth measured in other datasets, as it does for WASP-17b. Conclusions drawn about the atmospheric composition and temperature structure of exoplanets often depend on the occultation depths measured with IRAC. We warn that some of these may be unsound.

The WASP-17 system

WASP-17b is a 0.49-M_J, transiting planet in a 3.74-day, retrograde orbit around an F6V star (Anderson *et al.* 2010). The discovery paper data poorly constrain the orbital eccentricity ($0 < e < 0.31$), resulting in large uncertainties on the stellar (1.12 – 1.64 $R_\odot$) and planetary (1.41 – 2.07 R_J) radii. In the limit of the circular case, the planet radius takes the maximum value of 2.0 R_J. Triaud et al. (2010) place a tighter constraint on the eccentricity ($0.023 < e < 0.096$), but this is still insufficient to determine precisely the planet radius.

Observations and data analysis

Observations:

We observed two occultations of WASP-17b with *Spitzer*/IRAC, on 2009 Apr 24 (*ecl1*) and 2009 May 01 (*ecl2*). Each occultation was observed simultaneously at 4.5 and 8 μm (channels 2 & 4, respectively). The observations, each lasting 8.4 hours, were conducted in full-array mode with 10.4 s exposures. The detector target positions were pre-flashed to reduce the channel 4 'ramp' effect (Knutson *et al.* 2008).

Data analysis:

We performed aperture photometry with IRAF, using a range of circular apertures (1 – 6 pixels), centred by Gaussian PSF fitting and a sky b/g annulus with inner and outer radii of 8 and 12 pixels respectively. The photometric uncertainties are the quadrature sum of the sky background, readout and Poission noise. A timing correction was made to account for the light-travel time across the WASP-17b orbit.

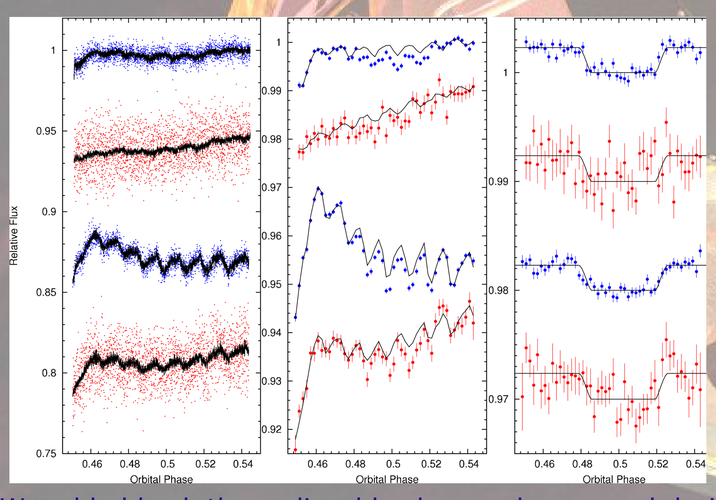

Fig. 1: Occultation photometry – the upper two lightcurves in each panel are ecl1 and the lower two are ecl2. 4.5 μm data are shown in blue and 8 μm data are in red. Left: Raw data with the best-fitting trend and occultation model superimposed. Middle: Binned data with the trend model. Right: Binned data divided by the best-fitting trend model, with the best-fitting eclipse model shown. The fluxes are normalised to unity during occultation and relative flux offsets are applied for clarity. The approximately hour-long, periodic variations in flux in each dataset are caused by intra-pixel sensitivity and the nodding of the spacecraft.

We added back the zodiacal background, removed during sky-dark subtraction, to the images in order to calculate accurately the photometric uncertainties (Reach *et al.* 2005), and to determine the optimal photometric aperture size.

We rejected 1-2% of data points as flux or detector position outliers. This rejection level is consistent with that expected due to cosmic rays / solar protons.

We then performed a global MCMC analysis (Collier Cameron *et al.* 2007) incorporating SuperWASP and Euler photometry, and CORALIE and HARPS radial velocities. The decorrelation of *Spitzer* lightcurves with time and detector position (next section) is done within our Monte-Carlo Markhov Chain (MCMC) analysis. Values of the trend model coefficients are determined at each MCMC step by linear least-squares minimisation. This is done using singular value decomposition after dividing by the eclipse model. We fit a common eclipse model to data from the same channel, but separate trend models to each dataset.

Spitzer/IRAC systematics

Spitzer/IRAC is known to suffer from the following systematic effects: (1) an intra-pixel sensitivity ('pixel-phase') effect in channels 1 (3.6 μm) & 2 and (2) a time-dependent sensitivity ('ramp') effect in channels 3 (5.8 μm) & 4.

Detrending systematics in channel 2 (4.5 μm):

We model the pixel-phase effect as a quadratic function of sub-pixel position of PSF centre (Charbonneau et al. 2008). This, together with a linear term in time, detrend the data well (Fig. 1). We find that the systematics are of a significantly lower amplitude in *ecl1* data than *ecl2*. This is due to a chance placement of the star on the detector. In *ecl1*, the motion of the star on the detector in *x* and *y* somewhat compensate each other, meaning the distance from pixel centre does not vary much. In *ecl2*, however, the *x* and *y* motions combine to produce large amplitude oscillations from pixel centre (Fig. 2).

Detrending systematics in channel 4 (8 μm):

We initially tried modelling the time-dependent 'ramp' with a function quadratic in ln(time) (Charbonneau et al. 2008). However, we noticed that the residuals to the best-fit exhibited periodic features very similar to those present in the corresponding channel 2 data (Fig. 3). We therefore tried detrending with target detector position, in addition to a linear function of time (as for channel 2). Including spatial detrending resulted in a better fit (smaller residuals about the fit and a lower Bayesian Information Criterion (BIC) value). Significantly, a shallower measured eclipse depth also resulted (Fig. 1). Together with the spatial function, we tried a variety of time-dependent functions; a linear function of time gave the lowest BIC value.

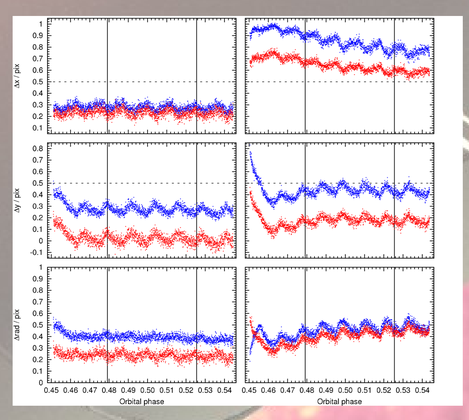

LEFT: Fig. 2: The distance of WASP-17 from the nearest pixel centre in the x, y, and radial directions (upper, middle and lower panels, respectively). Blue points correspond to 4.5 μm; red to 8 μm. Left: ecl1. Right: ecl2.

RIGHT: Fig. 3: Effect of neglecting the pixel-phase effect in our channel 4 data: 8 μm data detrended with a quadratic in ln(time) and no spatial components. Upper panel: binned data with trend model only. Lower panel: binned, de-trended data with eclipse model. In each panel ecl1 is the upper curve, and ecl2 the lower. The residuals here are much larger than when de-trending for position (Fig. 1).

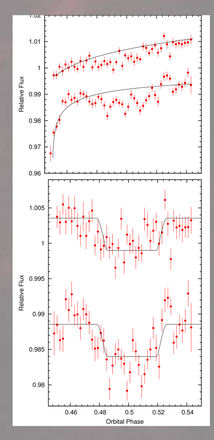

Photometric aperture size

We performed aperture photometry with a range of aperture radii (1-6 pixels) and chose the optimal values (4.5 μm: 2.9 pix, 8 μm: 1.6 pix) by maximising the target signal-to-noise (Fig. 4). The optimal channel 4 radius is smaller because the target is ~4 times fainter and the background ~20 times higher than in channel 2.

Due to the brightness of the target relative to the background at 4.5 μm, the fitted occultation depth is insensitive to the choice of aperture radius (Fig. 6, upper panel). However, at 8 μm the choice of aperture radius impacts the fitted occultation depth (Fig. 6, middle panel). If the pixel-phase effect is neglected, the fitted channel 4 occultation depth is unreliable (Fig. 6, lower panel).

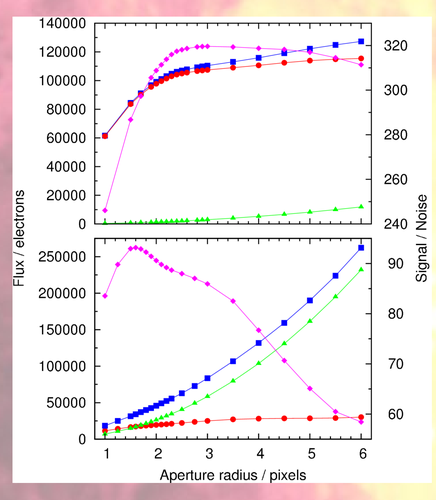

LEFT: Fig. 4: The flux due to WASP-17 (red), the background (green) and the total flux (blue) as a function of aperture radius. Also shown is the signal-to-noise ratio of the target (magenta). The upper panel is for the 4.5 μm data, while the lower panel is for the 8 μm data.

RIGHT: Fig. 5: The dependence on aperture radius of the fitted occultation depth (red) and the RMS of the residuals (ecl1: blue, ecl2: green) for the 4.5 μm data (upper panel), 8 μm when treating for pixel-phase (middle), and 8 μm when neglecting pixel-phase (lower).

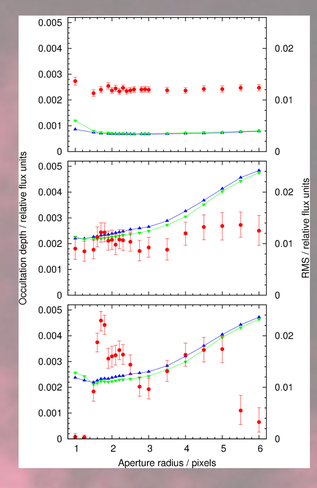

Results and conclusions

We have shown that the pixel-phase effect known to exist in IRAC channel 2 is also present in IRAC channel 4 (and, we suggest, probably in channel 3) and should be accounted for. It is also important to choose the optimal aperture radius, particularly when the target is faint relative to the background. Failure to do so can result in inaccurate occultation depths and unreliable conclusions.

The results of our global analysis of all available WASP-17 data are displayed in Fig. 6. With a radius of $2R_J$, WASP-17b is 0.7 R_J larger than predicted by a theoretical model of irradiated gas giant planets (Fortney et al. 2007). We are currently determining the implications of the occultation depths for the composition and temperature structure of the atmosphere of WASP-17b.

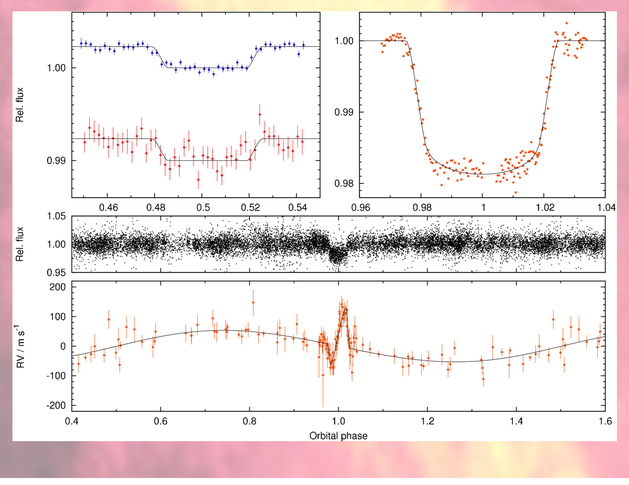

Fig. 6: Data and best-fitting models from our global MCMC analysis. Top-left: Spitzer/IRAC occultations at 4.5 (blue) and 8 (red) microns. Top-right: Euler transit photometry. Middle: SuperWASP photometry. Bottom: Radial velocities from HARPS and CORALIE.

References

Anderson *et al.* A&A **513**, L3 (2010)
Charbonneau *et al.* ApJ **686**, 1341 (2008)
Cameron *et al.* MNRAS **380**, 1230 (2007)
Fortney *et al.* ApJ **659**, 1661 (2007)
Knutson *et al.* ApJ **673**, 526 (2008)
Reach *et al.* PASP **117**, 978 (2005)
Triaud *et al.* A&A in press (2010)